INORGANIC CHEMISTRY FRONTIERS

RESEARCH ARTICLE

View Article Online
View Journal

Cite this: DOI: 10.1039/d6qi00856a

Binding azaphilic copper radioisotopes with all-nitrogen macrocycles for cancer theranostics

Sara Franchi,[a] Mattia Asti,[b] Nóra V. May,[c] Silvia Pozzo,[a] Sofia Gama,[d] Erika Ferrari,[e] Laura Pigani,[e] Christian Jentschel,[f] Christin Neuber,[f] Fabrizio Mancin,[a] Sven Stadlbauer,[f] Klaus Kopka,[f,g,h,i] Constantin Mamat,[f] Helmut Mäcke,[j] Valerio Di Marco[a] and Marianna Tosato *[k,l]

Copper radioisotopes constitute a true theranostic family, enabling cancer imaging and therapy with chemically identical metal-based radiopharmaceuticals. Developing chelators that provide copper complexes combining high thermodynamic stability, kinetic inertness, and redox robustness remains a key challenge. Herein, we investigated a cyclen-based chelator with aminoethyl side chains (1,4,7,10-tetraazacyclododecane-1,4,7,10-tetrakis(2-ethylamine), DO4N) and its TACN analogue (1,4,7-triazacyclononane-1,4,7-tris(2-ethylamine), NO3N). Both chelators rapidly form Cu^{2+} complexes with high thermodynamic stability comparable to or exceeding that of their carboxylate counterparts (DOTA and NOTA), with DO4N displaying superior stability. Cu^{2+} complexes adopt an elongated octahedral (DO4N) or distorted square pyramidal (NO3N) geometry in solution. All macrocyclic amines coordinate the metal, while only one or two side chains participate, leaving additional $-NH_2$ groups available for conjugation to biological vectors. Both ligands are also able to stabilize Cu^{+} upon reduction. Radiolabeling with $[^{64}Cu]Cu^{2+}$ demonstrated superior incorporation by both DO4N and NO3N compared to NODAGA under mild conditions, with DO4N achieving the highest labeling efficiency. Both $[^{64}Cu]Cu^{2+}$ complexes remained fully intact in human serum over 24 h. *In vivo* PET imaging with $[^{64}Cu]$Cu-DO4N showed sufficient stability for imaging, with renal clearance dominating early biodistribution. The results indicate that these all-nitrogen macrocycles are highly promising scaffolds for next-generation copper-based theranostic radiopharmaceuticals.

Received 22nd April 2026,
Accepted 8th May 2026

DOI: 10.1039/d6qi00856a

rsc.li/frontiers-inorganic

Introduction

Metal-based targeted radiopharmaceuticals represent powerful molecular tools in precision medicine, enabling the noninvasive visualization and treatment of cancer and other diseases at molecular level.[1] In these agents, metallic radionuclides are conjugated to a biologically active targeting vector, such as a small molecule, peptide, antibody, or protein, through a bifunctional chelator able to firmly bind the radiometal, to ensure the selective delivery of radioactivity to the desired biological target while preventing nonspecific off-target accumulation.[2] The chelator thus plays a central role in dictating the *in vivo* stability, pharmacokinetics, and overall biological performance of the radiopharmaceutical by warranting high thermodynamic stability and kinetic inertness *in vivo*, while ideally allowing rapid radiometal incorporation under mild pH and temperature.[2]

Owing to their favorable nuclear decay properties that enable both imaging and therapy, copper radioisotopes have attracted increasing attention for theranostic applications. The medium-energy β^- and γ emitter copper-67 (^{67}Cu, $t_{1/2}$ = 61.8 h) is suitable for β^- therapy and treatment monitoring, whereas

[a]Department of Chemical Sciences, University of Padova, 35131 Padova, Italy
[b]Radiopharmaceutical Chemistry Laboratory, Nuclear Medicine Unit, AUSL-IRCCS Reggio Emilia, 42122 Reggio Emilia, Italy
[c]Centre for Structural Sciences, HUN-REN Research Centre for Natural Sciences, 1117 Budapest, Hungary
[d]Center for Nuclear Sciences and Technologies, Instituto Superior Técnico, University of Lisbon, 2695-066 Bobadela, Portugal
[e]Department of Chemical and Geological Sciences, University of Modena and Reggio Emilia, 41125 Modena, Italy
[f]Institute of Radiopharmaceutical Cancer Research, Helmholtz-Zentrum Dresden-Rossendorf (HZDR), D-01328 Dresden, Germany
[g]TUD Dresden University of Technology, School of Science, Faculty of Chemistry and Food Chemistry, D-01062 Dresden, Germany
[h]German Cancer Consortium (DKTK), Partner Site Dresden, D-01307 Dresden, Germany
[i]National Center for Tumor Diseases (NCT), NCT/UCC Dresden, D-01307 Dresden, Germany
[j]Department of Nuclear Medicine, University Hospital Freiburg, D-79106 Freiburg, Germany
[k]Department of Chemistry, Simon Fraser University, Burnaby, V5A 1S6 British Columbia, Canada. E-mail: marianna_tosato@sfu.ca
[l]Life Sciences, TRIUMF, Vancouver, BC V6T 2A3 British Columbia, Canada

copper-60 (^{60}Cu, $t_{1/2}$ = 23.7 min), copper-61 (^{61}Cu, $t_{1/2}$ = 3.3 h), and copper-62 (^{62}Cu, $t_{1/2}$ = 9.7 min) emit positrons (β^+) and are suitable for positron emission tomography (PET) imaging.[3] The dual β^+–β^- emitter copper-64 (^{64}Cu, $t_{1/2}$ = 12.7 h) can be employed in PET procedures as well.[3,4] However, the clinical promise of copper-based radiopharmaceuticals is often compromised by *in vivo* radiometal release.

Copper exists in two biologically relevant oxidation states, Cu^{2+} and Cu^{+}, which exhibit distinct coordination preferences.[4,5] Cu^{2+} is a borderline-hard Lewis acid favoring nitrogen and oxygen donors, while Cu^{+}, being a soft cation, prefers sulfur and phosphorus ligands.[5,6] Although radiopharmaceuticals typically employ Cu^{2+} complexes, *in vivo* reduction to Cu^{+} can occur (E^0 = +0.15 V at 25 °C, *vs.* the normal hydrogen electrode – NHE), caused by endogenous reductants such as glutathione, nicotinamide adenine dinucleotide phosphate (NADPH), ascorbic acid, and hypoxic tumor environments (E^0 = −0.40 V *vs.* NHE).[7–9] This process promotes transchelation to Cu^{+}-binding biomolecules, leading to loss of radioactivity from the targeting vector.[4,10,11] Therefore, designing complexing agents capable of either preventing Cu^{2+} reduction or maintaining strong binding across both oxidation states is crucial for advancing next-generation copper-based theranostics.[12]

Over the years, a variety of chelators have been explored for the complexation of copper radioisotopes in the attempt to reach an optimal combination of simple synthesis, rapid radiolabeling, and *in vivo* stability. Polyazamacrocycles functionalized with carboxylate, phosphonate, pyridine, picolinic acid, or combinations thereof, dominate copper chelation strategies.[4,7,13,14] 1,4,7,10-Tetraazacyclododecane (cyclen) and 1,4,8,11-tetraazacyclotetradecane (cyclam) derivatives, such as 1,4,7,10-tetraazacyclododecane-1,4,7,10-tetraacetic acid (DOTA, Fig. 1) and 1,4,8,11-tetraazacyclotetradecane-1,4,8,11-tetraacetic acid (TETA), form Cu^{2+} complexes with high thermodynamic stability but often require harsh radiolabeling conditions and exhibit suboptimal *in vivo* stability.[15,16] Nonetheless, their commercial availability has enabled translation to the clinic, most notably in [^{64}Cu]Cu-DOTA-TATE (Detectnet™), approved by the US Food and Drug Administration (FDA) in 2020 for PET imaging of somatostatin receptor-positive neuroendocrine tumors.[17] Derivatives of the 1,4,7-triazacyclononane (TACN) scaffold, such as 1,4,7-triazacyclononane-1,4,7-triacetic acid (NOTA, Fig. 1) and ((7-(1-carboxy)-4-carboxybutyl)-1,4,7-triazacyclononane)-1,4-diacetic acid (NODAGA), provide faster radiolabeling under mild conditions maintaining excellent *in vivo* inertness, and are now widely established in copper radiopharmaceutical design.[18,19]

Despite these successes, there remains a need for next-generation chelators that can further improve coordination strength and redox stability. While most copper chelators rely on oxygen- or aromatic nitrogen-containing pendant arms, primary amine-rich systems remain scarcely explored, despite the strong affinity of copper for nitrogen donors. Actually, one of the most effective scaffolds for copper complexation so far is the hexaazamacrobicyclic sarcophagine (SAR), an all-nitrogen donor cage able to form extraordinarily stable copper complexes with good *in vivo* stability.[20–22]

Building on early work by Tei *et al.* on aminoethyl- and aminopropyl-functionalized TACN derivatives,[23] we turned our attention to all-nitrogen-containing macrocyclic chelators as an underexplored opportunity to enhance copper coordination. Specifically, we focused herein on the cyclen-based chelator 1,4,7,10-tetraazacyclododecane-1,4,7,10-tetrakis(2-ethylamine) (DO4N, Fig. 1) and its TACN-based analogue, 1,4,7-triazacyclononane-1,4,7-tris(2-ethylamine) (NO3N, Fig. 1) as novel ligands to complex copper radioisotopes. These compounds, characterized by primary amine-rich pendant arms, were envisioned to provide an ideal environment for stabilizing copper in both oxidation states through strong nitrogen coordination.

This study offers a comprehensive investigation of the chemical, radiochemical and biological behavior of the two all-nitrogen chelators DO4N and NO3N. DO4N was already introduced in the literature by Dai *et al.*, who used it as a synthetic intermediate,[24] but its purification, characterization, as well as any applications have remained unreported so far. Therefore, for DO4N, we describe the synthesis, acid-base properties, and the kinetic, thermodynamic, and structural aspects of its Cu^{2+} and Cu^{+} complexes. In parallel, NO3N was revisited to extend the understanding of its coordination chemistry beyond the aspects previously reported by Tei *et al.*[23] To elucidate structure-property relationships, both chelators were systematically compared to their carboxylate counterparts, DOTA and NOTA. A multidisciplinary approach combining electrochemical

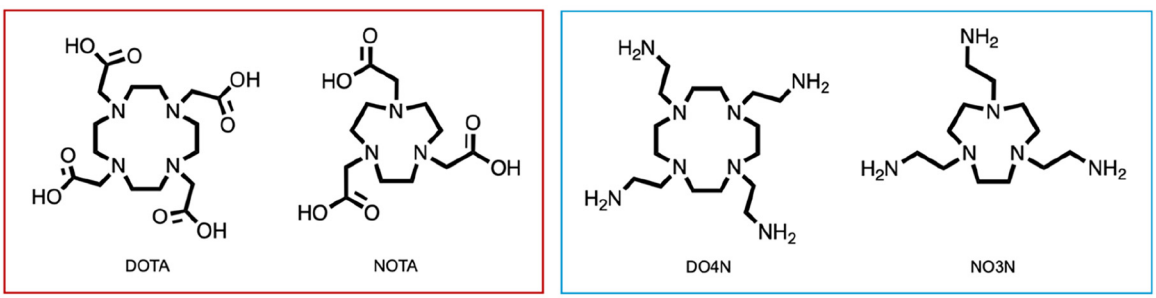

Fig. 1 Structures of carboxylate-containing cyclen- and TACN-based polyazamacrocycles, DOTA and NOTA, and all-nitrogen polyazamacrocycles investigated in this work, DO4N and NO3N.

(potentiometry and cyclic voltammetry), spectroscopic (UV-Vis, NMR, EPR), and X-ray diffraction analyses with radiochemical studies, including [^{64}Cu]Cu^{2+} radiolabeling, *in vitro* stability assays, and *in vivo* PET imaging, enabled a detailed understanding of how donor composition and macrocyclic architecture govern copper complex stability and *in vivo* behavior.

Results and discussion

Synthesis of all-nitrogen macrocycles

The precursor of the aminoethyl side arm was synthesized by protecting 2-chloroethylamine (**1**) with *tert*-butyloxycarbonyl (Boc) group (Fig. 2). The protected side chain (*tert*-butyl-*N*-(2-chloroethyl)carbamate, **3**) was subsequently employed to fully functionalize the secondary amines of cyclen (**4**) and TACN (**7**) macrocycles *via* nucleophilic substitution, obtaining DO4N-Boc (**5**) and NO3N-Boc (**8**), respectively. Final deprotection with HCl yielded the hydrochloride salts of the target chelators, DO4N·8HCl (**6**, 54% overall yield) and NO3N·6HCl (**9**, 55% overall yield). The identity and purity of all intermediates and final compounds were confirmed by multinuclear NMR spectroscopy (^{1}H, ^{13}C{^{1}H}, bidimensional NMR) and high-resolution mass spectrometry (HR-MS) (Fig. S1–S15).

Notably, attempts to synthesize DO4N through alkylation with a haloacetamide or a haloacetonitrile followed by reduction to the primary amine, as reported by Tei *et al.* for NO3N,[23,25] were not successful due to incomplete reduction. A similar synthesis of DO4N as that described herein was performed by Dai *et al.*, who reported "very low yields" and thus adopted a different strategy, which however gave a 21% yield.[24] Moreover, our synthetic pathway to obtain NO3N required shorter reaction times and lower temperatures compared to the synthesis by Tei *et al.*,[25] with a higher yield (55% *vs.* 45%, respectively).

Acid-base properties of all-nitrogen macrocycles

The acidity constants (pK_a) of DO4N were determined in aqueous solution by pH-potentiometry and complemented by pH-dependent ^{1}H NMR titrations (Fig. S16 and S17). The pK_a values of DO4N, alongside the literature values for NO3N for comparison purposes,[23] are listed in Table 1. The corresponding distribution diagrams are shown in Fig. S18, highlighting that under physiological conditions both ligands predominantly exist in their tri-protonated form, H_3L^{3+} (L denotes the deprotonated, neutral form of either DO4N or NO3N, as shown in Fig. 1).

Only six of the eight possible acidity constants for DO4N were identified (Table 1), likely because the first two are ≪2 due to strong electrostatic repulsion in highly protonated H_8L^{8+} and H_7L^{7+} species. The assignment of each pK_a of DO4N to either a tertiary amine within the macrocyclic ring or a primary amine on the pendant arms was inferred from ^{1}H NMR, based on which signals showed the largest chemical shift changes as a function of pH (Fig. S17). The first two pK_a correspond to the macrocyclic amines, while the remaining four are associated with the $-NH_3^+/-NH_2$ groups on the side

Table 1 Acidity constants (pK_a) of DO4N determined by pH-potentiometry at I = 0.15 M NaCl and T = 25 °C. Data for NO3N were taken from the literature[23] and are reported for comparison

Equilibrium[a]	DO4N		NO3N[b]	
$H_6L^{6+} \rightleftharpoons H_5L^{5+} + H^+$	1.8 ± 0.1	Ring	n.d.	Ring
$H_5L^{5+} \rightleftharpoons H_4L^{4+} + H^+$	2.6 ± 0.1	Ring	2.43	Ring
$H_4L^{4+} \rightleftharpoons H_3L^{3+} + H^+$	5.69 ± 0.09	Arm	5.16	Ring
$H_3L^{3+} \rightleftharpoons H_2L^{2+} + H^+$	8.67 ± 0.02	Arm	8.72	Arm
$H_2L^{2+} \rightleftharpoons HL^+ + H^+$	9.92 ± 0.03	Arm	9.52	Arm
$HL^+ \rightleftharpoons L + H^+$	11.23 ± 0.05	Arm	10.77	Arm

[a] L denotes the ligand in its completely deprotonated (neutral) form as shown in Fig. 1. [b] I = 0.1 M NMe_4Cl, T = 25 °C, data taken from ref. 23. n.d.: not determined under the adopted experimental conditions.

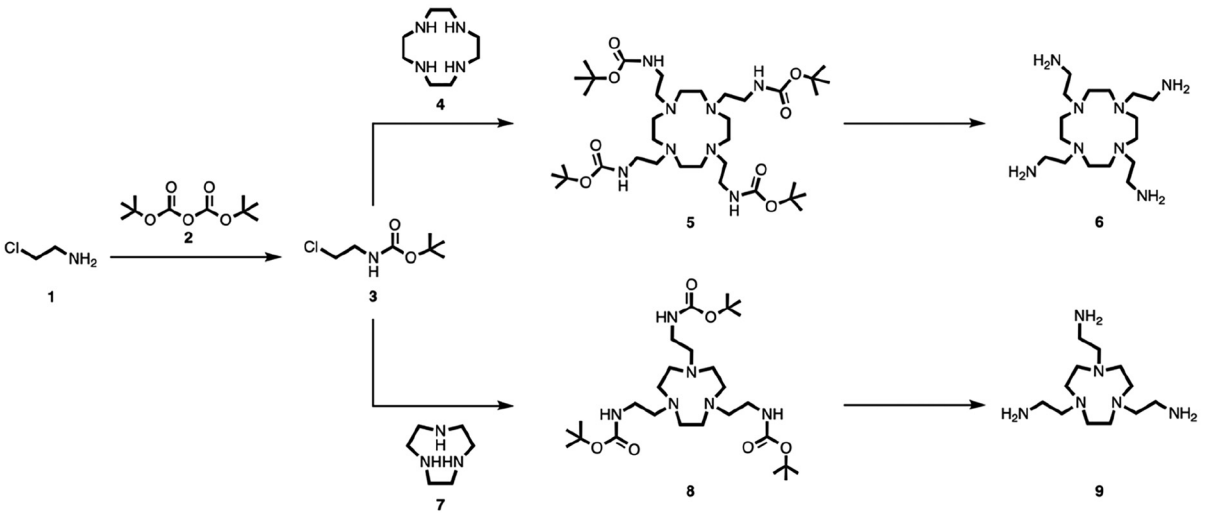

Fig. 2 Synthesis of DO4N (**6**) and NO3N (**9**).

arms. This deprotonation pattern (firstly the ring amines, then those on the side arms) closely mirrors that of NO3N, with both chelators displaying nearly identical acidity constant values, differing by maximum 0.5 logarithmic units (Table 1).

The analysis of the ^{1}H NMR spectra further reveals that DO4N maintains a D_{4h} symmetry across the examined pH range and that the equilibria between all the differently protonated forms of DO4N are fast compared to the NMR time scale, producing a single set of averaged signals.

Speciation and thermodynamic stability of Cu^{2+} complexes with all-nitrogen macrocycles

Before assessing the thermodynamic stability of the Cu^{2+} complexes of DO4N and NO3N, their formation kinetics were qualitatively explored by UV-Vis spectroscopy, since thermodynamic measurements require the system to be at equilibrium. The rate of both Cu^{2+}-DO4N and Cu^{2+}-NO3N formation is strongly pH- and reagent concentration-dependent, being faster when either of these two experimental parameters is increased. Additional details are given in the SI.

A combination of complementary techniques was employed to elucidate the speciation and determine the stability constants of Cu^{2+}-DO4N, due to the complexity of this metal-chelator system. Acid-base pH-potentiometry was used to investigate the pH range above 3, where the formation kinetics are sufficiently fast (see SI). This analysis revealed the presence of differently protonated complexes along with quantitative Cu^{2+} binding. Conversely, the slow kinetics observed below pH 3 precluded the use of pH-potentiometry in this pH range. To overcome this limitation, the speciation at pH < 3 was studied by variable-pH UV-Vis titrations, including highly acidic conditions, and UV-Vis competition experiments with cyclen. Representative spectra are reported in Fig. S25 and S26. In particular, the competition experiments enabled the calculation of the overall stability constants ($\log\beta$) of Cu^{2+}-DO4N complexes, using the known value for $[Cu(cyclen)]^{2+}$ from the literature[26] and the pK_a of both chelators (Table 1 for DO4N, ref. 27 for cyclen).

Four distinct complexes were identified, all exhibiting a 1 : 1 Cu^{2+}-to-DO4N stoichiometry and differing by a single proton, ranging from $[Cu(H_2DO4N)]^{4+}$ to $[Cu(DO4N)(OH)]^{+}$. This is the most probable speciation obtained by testing several models during titration fitting, which was supported by complementary techniques (*e.g.*, UV-Vis and EPR). The stability constants of Cu^{2+}-DO4N are collected in Table 2 while the corresponding distribution diagram is shown in Fig. 3A and compared with the data reported in the literature for Cu^{2+}-NO3N (Table 2, Fig. 3B).[23] Based on these results, the predominant forms under physiological conditions are $[Cu(DO4N)]^{2+}$ and $[Cu(HNO3N)]^{3+}$.

Highly charged species, such as $[Cu(H_2DO4N)]^{4+}$ and $[Cu(HDO4N)]^{3+}$, have also been previously observed for NO3N.[23] This can be rationalized by considering the protonation of uncoordinated aminoethyl side arms, which extend away from the metal center and reduce electrostatic repulsion with Cu^{2+}.

The presence of the hydroxo complex, $[Cu(DO4N)(OH)]^{+}$, suggests that water can also be involved in Cu^{2+} coordination sphere. This behavior was also noted for the aminopropyl-functionalized TACN derivative by Tei *et al.*[23]

Mass spectrometry further supported the 1 : 1 Cu^{2+}-to-DO4N stoichiometry (Fig. S27), since only signals arising from $[CuCl(DO4N)]^{+}$ could be detected (m/z: 442.2334 and 444.2310 – found; 442.24 and 444.23 – calc. for $[C_{16}H_{40}ClCuN_8]^{+}$).

The overall thermodynamic stability of the Cu^{2+} complexes with the all-nitrogen chelators (DO4N and NO3N) was compared to that of the corresponding carboxylic acid analogues (DOTA and NOTA) by calculating the pCu^{2+} value (Table 2), *i.e.* $pCu^{2+} = -\log[Cu^{2+}]_{free}$ at equilibrium under specific conditions. All the considered chelators form highly stable Cu^{2+} complexes. NOTA and NO3N exhibit equal overall stability, while DOTA binds Cu^{2+} 100-fold less strongly. Notably, the Cu^{2+} complexes of DO4N are markedly more stable than both their DOTA counterparts and the TACN derivatives, exceeding by 4 and 2 orders of magnitude the stability of the DOTA and NOTA/NO3N derivatives, respectively. This remarkable enhancement in thermodynamic stability reveals that replacing carboxylic pendants with amines on a cyclen scaffold significantly favors the complexation of Cu^{2+}, as postulated based on the known affinity of this metal to nitrogen donors.[5] From a biological perspective, the high pCu^{2+} of DO4N suggests that, at least thermodynamically, these complexes would be exceptionally resistant to dissociation under physiological conditions, minimizing the risk of copper release *in vivo*.

Table 2 Stability constants ($\log\beta$) of Cu^{2+}-DO4N determined by pH-potentiometry (unless otherwise stated) at I = 0.15 M NaCl and T = 25 °C. Data for NO3N, DOTA, and NOTA were taken from the literature[23,28] and are reported for comparison. The corresponding pCu^{2+} values were computed at $C_L = 10^{-5}$ M, $C_{Cu} = 10^{-6}$ M, pH = 7.4, by taking pK_a values from either Table 1 or literature data.[23,28] Formation of Cu^{2+} hydroxides resulted negligible under these conditions

Equilibrium[a]	DO4N	NO3N[b]	DOTA[c]	NOTA[d]
$Cu^{2+} + 2H^+ + L^n \rightleftharpoons [CuH_2L]^{(4-n)+}$	38.2 ± 0.2[e]	34.9	30.15	—
$Cu^{2+} + H^+ + L^n \rightleftharpoons [CuHL]^{(3-n)+}$	33.17 ± 0.04	31.5	26.6	24.37
$Cu^{2+} + L^n \rightleftharpoons [CuL]^{(2-n)+}$	27.07 ± 0.07	22.0	22.3	21.63
$Cu^{2+} + L^n + H_2O \rightleftharpoons [CuL(OH)]^{(1-n)+} + H^+$	18.5 ± 0.1	—	—	—
pCu^{2+}	20.4	18.3	16.5	18.3

[a] L^n denotes the ligand in its completely deprotonated form (*i.e.*, L for DO4N and NO3N, L^{4-} for DOTA, L^{3-} for NOTA). [b] I = 0.1 M NMe_4Cl, T = 25 °C, data taken from ref. 23. [c] I = 0.1 M NMe_4NO_3/Cl, T = 25 °C, data taken from ref. 28. [d] I = 1 M $NaClO_4$, T = 25 °C, data taken from ref. 28. [e] Determined by UV-Vis competition with cyclen.

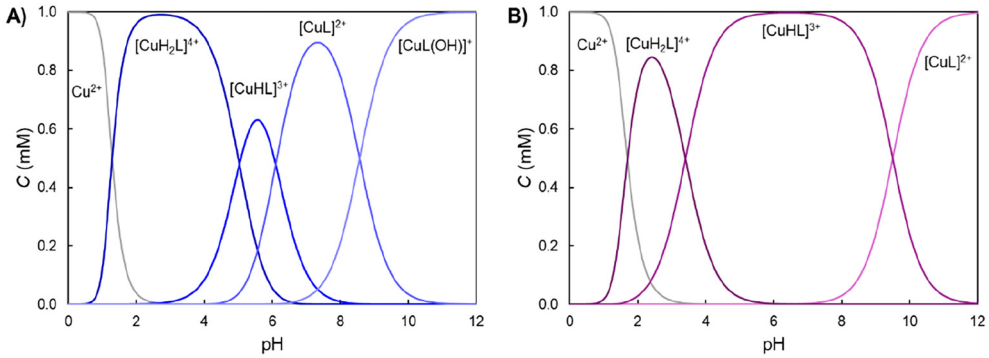

Fig. 3 Distribution diagram of (A) Cu^{2+}-DO4N and (B) Cu^{2+}-NO3N ($C_{Cu} = C_L = 10^{-3}$ M). Data for Cu^{2+}-NO3N were taken from the literature.[23]

Structure of Cu^{2+} complexes with all-nitrogen macrocycles in aqueous environment

The structural properties of the Cu^{2+} complexes with DO4N and NO3N in aqueous solution were explored by EPR and UV-Vis spectroscopies.

Variable-pH EPR spectra were acquired both at room temperature and in frozen state at 77 K (Fig. 4). In both cases, the spectra were relatively broad, and no superhyperfine splitting due to the coordinated nitrogen atoms was detected, even in frozen solution. Spectra of the single species composing each Cu^{2+}-chelator system were computed during the fitting process and are shown in Fig. S28 (77 K) and Fig. S29 (RT).

For Cu^{2+}-DO4N, two main spectral changes were observed at both room and low temperature. Both alterations are relatively modest, suggesting that they correspond to deprotonation events rather than to a complete modification of the coordination environment. The first spectral variation (pH ~ 4.5–5) is attributed to the equilibrium between $[Cu(H_2DO4N)]^{4+}$ and $[Cu(HDO4N)]^{3+}$, consistently with the species distribution curves (Fig. 3A). No marked spectral changes were detected around pH 6–7, where the deprotonation of $[Cu(HDO4N)]^{3+}$ to form $[Cu(DO4N)]^{2+}$ is expected, suggesting that $[Cu(DO4N)]^{2+}$ does not differ significantly in structure from $[Cu(HDO4N)]^{3+}$. This could be possible if the deprotonation of $[Cu(HDO4N)]^{3+}$ involves one non-coordinating side chain without modifying

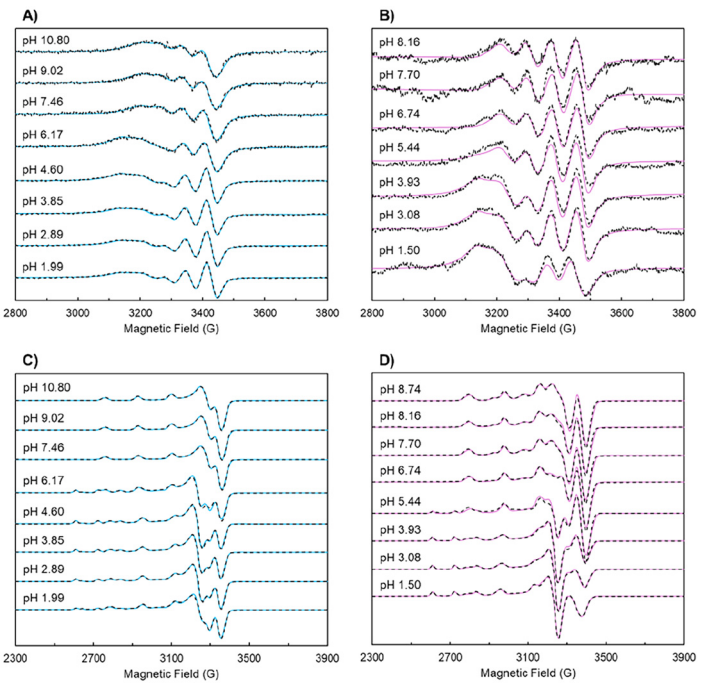

Fig. 4 Room temperature EPR spectra of (A) Cu^{2+}-DO4N and (B) Cu^{2+}-NO3N (H_2O, 9.54 GHz, T = 298 K, I = 0.15 M NaCl, $C_L = 2.2 \times 10^{-3}$ M, $C_{Cu} = 2.0 \times 10^{-3}$ M). Frozen solution EPR spectra of (C) Cu^{2+}-DO4N and (D) Cu^{2+}-NO3N (80% H_2O + 20% CH_3OH, 9.54 GHz, T = 77 K, I = 0.15 M NaCl, $C_L = 2.2 \times 10^{-3}$ M, $C_{Cu} = 2.0 \times 10^{-3}$ M). Both experimental (black dashed line) and simulated (colored solid line) spectra are shown.

the coordination environment around the Cu^{2+} ion. The second spectral variation (pH ~ 9) corresponds to the formation of $[Cu(DO4N)(OH)]^{+}$ in alkaline solution.

EPR parameters (Table 3) indicate an axial *g*-tensor symmetry for all species, consistent with either an elongated octahedral (due to Jahn–Teller distortion) or a square pyramidal coordination environment around the Cu^{2+} ion. Since the EPR parameters are similar across the different species, this suggests that they share a comparable coordination geometry and donor set. We thus hypothesize that in all the DO4N complexes Cu^{2+} is likely coordinated in a six-coordinate mode, with four equatorial ring nitrogen atoms, one apical side chain, and an apical H_2O/OH^- ($[4N]N_{ax}O_{ax}$) (Fig. S32A). The differences among the four complexes are related to the protonation state of either the apical groups or the remaining side chains.

The electronic spectra of Cu^{2+}-DO4N at acidic pH (pH < 4.5) are dominated by a strong absorption band in the UV region with a maximum at λ_{max} 314–316 nm (molar extinction coefficient ε_{max} ~ 3.2–3.4 × 10^3 L mol^{-1} cm^{-1} depending on pH, as determined from Lambert–Beer's law, Fig. 5A). This band is attributed to N-to-Cu ligand-to-metal charge transfer (LMCT) transitions, consistent with previous observations for other Cu^{2+}-cyclen derivatives.[27] In the same pH range, a weaker band at λ_{d-d} ~ 693 nm (ε_{d-d} ~ 3.6–3.7 × 10^2 L mol^{-1} cm^{-1}) is observed, arising from d–d orbital transitions of the Cu^{2+} ion, imparting a bright light blue color to the solution (Fig. S30A and B). As the pH increases and deprotonated Cu^{2+}-DO4N complexes form, both absorption bands blue-shift by around 40 nm (Fig. 5A). At neutral-to-basic pH, the N-to-Cu LMCT band appears at λ_{max} = 271 nm (ε_{max} ~ 3.4 × 10^3 L mol^{-1} cm^{-1}). The absence of asymmetry in the band of $[Cu(DO4N)]^{2+}$ compared to $[Cu(DOTA)]^{2-}$ (Fig. S31 and Table S1) suggests a lower degree of distortion of the octahedral environment.[29,30] Moreover, the d–d transition shifts to λ_{d-d} ~ 654 nm with a very low molar extinction coefficient (ε_{d-d} ~ 70 L mol^{-1} cm^{-1}), resulting in a faintly colored solution (Fig. S30C). This change is attributed to deprotonation of the axial donor groups, which modifies the electronic environment around Cu^{2+}.

Notably, the position of the d–d band of Cu^{2+}-DO4N complexes is comparable to those previously reported for cyclen, DOTA and 1,7-bis[2-(methylsulfanyl)ethyl]-4,10-diacetic acid-1,4,7,10-tetraazacyclododecane (DO2A2S) ($[4N]H_2O_{ax}$, $[3N,O]N_{ax}$, $[2N,2O]2N_{ax}$, respectively), further supporting an octahedral coordination mode with a mix of N and O donors in the coordination sphere (Table S1).[27]

The solution structure of Cu^{2+}-NO3N was investigated to complement the characterization of this system. EPR spectra (Fig. 4) confirmed the presence of the complexes previously detected by Tei *et al.*[23] A protonated species, $[Cu(H_2NO3N)]^{4+}$, was identified in strongly acidic solutions, both at RT and in frozen samples. Around neutrality (6 < pH < 8), the predominant complex, $[Cu(HNO3N)]^{3+}$, is characterized by a highly rhombic geometry. This suggests the equatorial coordination

Table 3 Isotropic (RT) and anisotropic (77 K) EPR parameters obtained for the species identified in Cu^{2+}-DO4N system. Errors are ±0.001 for *g* and ±1 × 10^{-4} cm^{-1} for *A* values

Species	Isotropic parameters		Anisotropic parameters				Calculated
	g_0	A_0 [a]	$g_\perp$	$g_\parallel$	$A_\perp$ [a]	$A_\parallel$ [a]	$g_{0,calc}$ [b]
$Cu^{2+}_{(aq)}$	2.196	35	2.081	2.423	15	126	2.195
$[CuCl]^{+}$			2.068	2.380	17	139	2.172
$[Cu(H_2DO4N)]^{4+}$	2.112	64	2.050	2.221	18	167	2.107
$[Cu(HDO4N)]^{3+}$/$[Cu(DO4N)]^{2+}$	2.115	61	2.049	2.235	19	176	2.111
$[Cu(DO4N)(OH)]^{+}$	2.115	57	2.050	2.239	19	171	2.113

[a] *A* values are reported in 10^{-4} cm^{-1} units. [b] Calculated as the average of $g_\perp$ and $g_\parallel$.

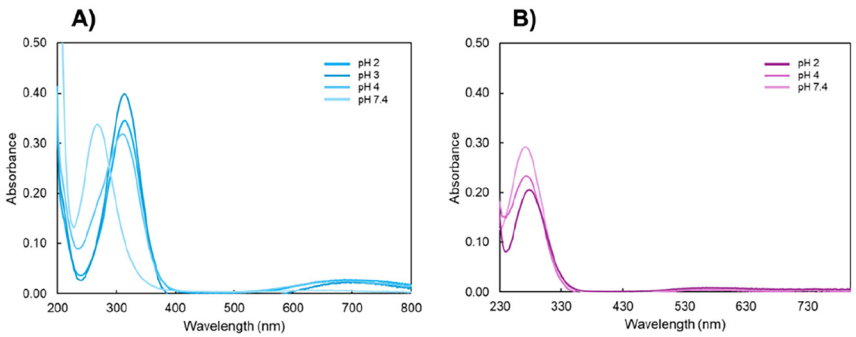

Fig. 5 UV-Vis spectra of (A) Cu^{2+}-DO4N and (B) Cu^{2+}-NO3N at selected pH values (C_{Cu} = C_L = 10^{-4} M, *T* = 25 °C). Spectra were acquired also at C_L = 10^{-3} M to accurately calculate the molar extinction coefficients of d–d bands (see text).

of two ring and two side-chain amino groups and the axial coordination of the third ring nitrogen in a distorted square pyramid, where the Cu^{2+} ion is slightly above the equatorial plane (Fig. S32B), in agreement with the solid-state structure proposed by Tei *et al.*[23] The isotropic (RT) spectrum of $[Cu(HNO3N)]^{3+}$ was also well described by fitting the rotational correlation time using the anisotropic parameters, confirming that the geometry detected at 77 K is identical to that present at room temperature. At higher pH a third complex, $[CuNO3N]^{2+}$, was detected in frozen solution with an increase in g_z that indicates a weakening of the ligand field in the equatorial plane (Table 4). This spectral change can be interpreted as a strengthening of the Cu–N_{ax} bond, which occurs when the last side-chain amino group bound to this ring nitrogen is deprotonated. Thus, we suggest that deprotonation does not cause geometric rearrangement compared to $[Cu(HNO3N)]^{3+}$.

The UV-Vis spectrum of Cu^{2+}-NO3N solutions is largely independent of pH in the acidic-to-neutral range (pH ≤ 7.4), indicating that $[Cu(H_2NO3N)]^{4+}$ and $[Cu(HNO3N)]^{3+}$ likely have a similar coordination environment (Fig. 5B). The LMCT transition (λ_{max} ~ 276–280 nm, ε_{max} ~ 2.0–3.0 × 10^3 L mol^{-1} cm^{-1}) closely matches those previously reported for Cu^{2+} complexes with TACN derivatives such as TACN-*n*-Bu and NO3S,[31] and is slightly red-shifted respect to those of Cu^{2+}-TACN and Cu^{2+}-NOTA (Fig. S33), supporting its attribution to N-to-Cu transitions.

By contrast, the d–d transition appears at an unusually low wavelength (λ_{d-d} ~ 567–573 nm, ε_{d-d} ~ 1.0–1.3 × 10^2 L mol^{-1} cm^{-1}), imparting a peculiar lilac color to Cu^{2+}-NO3N solutions (Fig. S30D–F). This feature was observed also for other Cu^{2+} complexes like $[Cu(ethylenediamine)_2(H_2O)]I_2$ and $[Cu(CN)_4(HCN)]$ by Glasner and Asher, who conjectured that violet color might be typical of penta-coordinated Cu^{2+} species.[32] This hypothesis appears valid also for Cu^{2+}-NO3N, consistent with the distorted square pyramidal geometry deduced from EPR. This coordination explains why both EPR and UV-Vis spectra and parameters of $[Cu(HNO3N)]^{3+}$ markedly differ from those of the octahedral complexes such as $[Cu(TACN)(H_2O)_3]^{2+}$, [Cu(HNOTA)], $[Cu(NOTA)]^{-}$, and $[Cu(NO3S)]^{2+}$ (Table S1 and Fig. S33).[30,31,33]

Solid-state structure of Cu^{2+}-DO4N

Crystals of Cu^{2+}-DO4N suitable for single-crystal X-ray diffraction were obtained from a water/ethanol solution. The summary of data collection and refinement parameters for $[Cu(H_2DO4N)Cl]Cl_3$ + solvent (10) are collected in Table S2 and the ORTEP representation of the complex is shown in Fig. 6.

In the crystal structure, Cu^{2+} is coordinated equatorially by the four nitrogen atoms of the macrocyclic ring and axially by one chloride counter ion. The ligand adopts two types of disordered conformations with 0.50/0.50 occupancy, and, due to symmetry, two side chains further split into two positions with 0.25/0.25 occupancy, resulting in high uncertainty in the atomic positions. From one conformer to the other, the macrocyclic ligand rotates by ~15° around the axial Cu–Cl bond, and the five-member Cu–N–C–C–N chelate rings flip from the δδδδ (molecule 1) to the λλλλ (molecule 2) conformation and *vice versa*. The complex is cut by a symmetry plane, so half of the complex is located in the asymmetrical unit (Fig. S34).

Since the ligand exhibits complete disorder and assignment of the peripheral atoms remains ambiguous, the structural analysis is herein limited to the connectivity of the complex, whereas additional considerations are available in the SI. Consequently, the derived bond lengths and angles are subject to significant uncertainty and should be interpreted with caution. A similar profile with one disordered pendant arm was highlighted also for $[Cu(NO3N)]^{2+}$.[23] While the solid-state structure shows a preference for coordination of an apical chloride, solution data indicate coordination of a nitrogen donor from a side chain along with a water molecule (see above). Differences between solid-state and solution behavior are common and well documented in the literature.[27,30,34]

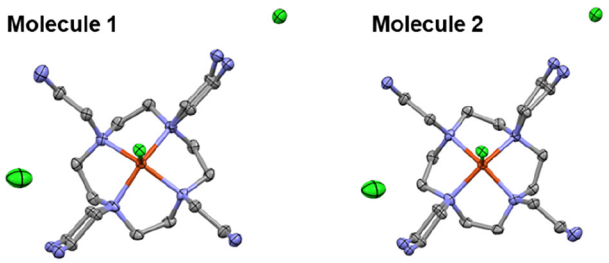

Fig. 6 ORTEP representation of the two conformations (molecule 1 and molecule 2, chemical occupancy ratio 0.50/0.50) of the complex in the crystal $[Cu(H_2DO4N)Cl]Cl_3$ + solvent. Two side chains are further split into two positions (0.25/0.25 occupancy) along a symmetry plane. Displacement parameters are drawn at 50% probability level.

Table 4 Isotropic (RT) and anisotropic (77 K) EPR parameters obtained for the species in Cu^{2+}-NO3N system. Errors are ±0.001 for *g* and ±1 × 10^{-4} cm^{-1} for *A* values

Species	Isotropic parameters		Anisotropic parameters						Calculated
	g_0	A_0 [a]	g_x	g_y	g_z	A_x [a]	A_y [a]	A_z [a]	$g_{0,calc}$ [b]
$Cu^{2+}_{(aq)}$	2.194	36	2.084	2.084	2.421	6	6	127	2.196
$[Cu(H_2NO3N)]^{4+}$	2.102	72	2.040	2.040	2.213	17	17	173	2.098
$[Cu(HNO3N)]^{3+}$	2.096	75	2.033	2.061	2.194	5	49	176	2.096
$[Cu(NO3N)]^{2+}$			2.059	2.059	2.243	10	10	154	2.120

[a] *A* values are reported in 10^{-4} cm^{-1} units. [b] Calculated as the average of g_x, g_y and g_z.

Notably, comparison of the spectroscopic parameters of Cu^{2+}-DO4N with those of Cu^{2+}-cyclen and Cu^{2+}-DOT-*n*-Bu (DOT-*n*-Bu is 1,4,7,10-tetra-*n*-butyl-1,4,7,10-tetraazacyclododecane)[27] indicates that, if only the macrocyclic nitrogens were involved in both complexes, similar parameters would be expected. The observed differences, together with radiochemical and biological data (*vide infra*), provide strong evidence for the active involvement of the side chains in solution, underscoring their crucial role in stabilizing the metal center. Biological data (see below), provide strong evidence for the active involvement of the side chains in solution, underscoring their crucial role in stabilizing the metal center.

Cu^{+} binding with all-nitrogen macrocycles

Cyclic voltammetry (CV) was used to investigate the redox behavior of Cu-DO4N and Cu-NO3N. As shown in Fig. 7, both systems exhibited two well-defined peaks assigned to the Cu^{2+}/Cu^{+} redox couple at physiological pH. The voltametric response did not change with time or after multiple reduction/oxidation cycles, indicating that no Cu loss occurs upon reduction.

Peak current increased with scan rate as expected, while both complexes showed quasi-reversible behavior (ΔE_p > 60 mV). For Cu-DO4N, ΔE_p remained nearly constant (141–151 mV) regardless of the scan rate, suggesting relatively slow but consistent electron transfer kinetics. In contrast, Cu-NO3N showed a pronounced dependence of ΔE_p on scan rate (*e.g.*, ΔE_p = 94 mV at 5 mV s^{-1} and ΔE_p = 181 mV at 200 mV s^{-1}), which indicates a slower electron transfer process likely coupled to structural reorganization following reduction. The voltametric results demonstrate that both ligands can stabilize Cu in both oxidation states, and that the pre-formed Cu^{2+} complexes remain intact upon reduction on the time scale of CV experiments.

The reduction potentials ($E_{1/2}$) at physiological pH ($E_{1/2,\ Cu\text{-}DO4N}$ = −0.21 V *vs.* NHE and $E_{1/2,\ Cu\text{-}NO3N}$ = +0.27 V *vs.* NHE) are more positive than the standard reduction potential of common biological reductants (E^0 = −0.40 V *vs.* NHE), implying that *in vivo* reduction of the Cu^{2+} complexes is thermodynamically feasible and more favored for Cu^{2+}-NO3N than for Cu^{2+}-DO4N (since $E_{1/2,\ Cu\text{-}NO3N} \gg E_{1/2,\ Cu\text{-}DO4N}$). However, the voltammetric data show that both DO4N and NO3N efficiently stabilize Cu^{+}, preventing demetallation upon reduction. Similar properties were previously found for sulfur-rich macrocyclic chelators and sarcophagine derivatives, where the presence of sulfur and/or nitrogen donors stabilized the Cu^{+} complexes,[27,31,35–37] whereas irreversibility of CV patterns due to the release of Cu^{+} from carboxylate-bearing chelators like TETA and DOTA is well-known.[11,16]

$[^{64}Cu]Cu^{2+}$ radiolabeling of all-nitrogen macrocycles

Concentration-, pH-, and temperature-dependent radiolabeling of DO4N, NO3N and NODAGA (reference) with $[^{64}Cu]Cu^{2+}$ were conducted (Fig. 8). Representative radio-TLC and a radio-HPLC chromatogram of DO4N and NO3N radiolabeling reactions are reported in Fig. S37 and S38.

The radiolabeling performance of NODAGA was unaffected by pH or temperature, achieving quantitative $[^{64}Cu]Cu^{2+}$ radiochemical incorporation (RCI) at $C_L \geq 10^{-5}$ M. In contrast, DO4N and NO3N displayed markedly superior radiolabeling efficiencies.

At pH 4.5, NO3N achieved quantitative $[^{64}Cu]Cu^{2+}$ labeling (>95%) at $C_L \geq 10^{-5}$ M and maintained high incorporation (>82%) even at $C_L = 10^{-6}$–10^{-7} M at room temperature. Heating further enhanced radiolabeling efficiency, lowering the threshold for quantitative incorporation to $C_L = 10^{-7}$ M (Fig. 8). DO4N outperformed both NO3N and NODAGA, enabling quantitative binding of $[^{64}Cu]Cu^{2+}$ at extremely low concentrations (down to $C_L = 10^{-8}$ M), with no significant temperature dependence (Fig. 8). Such a low concentration of chelator indicates an outstanding radiolabeling ability as the DO4N-to-$[^{64}Cu]Cu^{2+}$ molar ratio corresponds to 3–5/1 under optimal conditions, whereas NODAGA required a 3–5 × 10^3/1 ratio at best to reach full incorporation. These results highlight the exceptional radiolabeling ability of DO4N and NO3N. At pH 7, NO3N achieved quantitative labeling at $C_L \geq 10^{-6}$ M and DO4N at $C_L \geq 10^{-7}$ M, at both room and high temperature (Fig. 8). Thus, both chelators significantly outperformed NODAGA, with DO4N again demonstrating a higher efficiency than NO3N. The slightly diminished radiolabeling performance at pH 7 compared to pH 4.5 could be justified by the possible formation of competitive species, such as Cu^{2+} hydroxides and phosphates, since phosphate buffered saline (PBS) was used as buffer.

Overall, both chelators enable highly efficient $[^{64}Cu]Cu^{2+}$ radiolabeling under mild conditions, making them suitable for conjugation to a wide range of biomolecules.

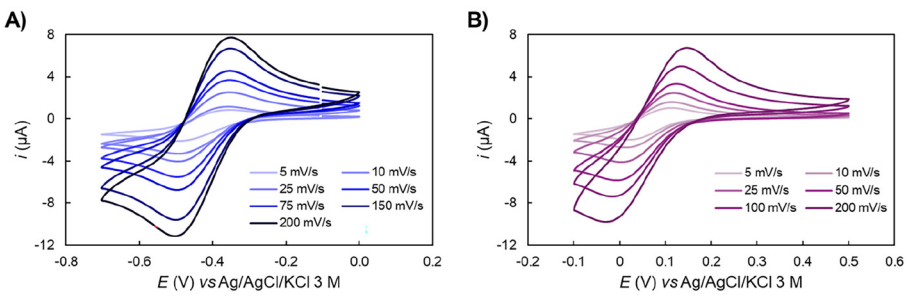

Fig. 7 Cyclic voltammograms of copper complexes with (A) DO4N and (B) NO3N (C_{Cu} = 1.0 × 10^{-3} M, C_L = 1.2 × 10^{-3} M, T = 25 °C, I = 0.15 M $NaNO_3$ in H_2O, pH 7.4).

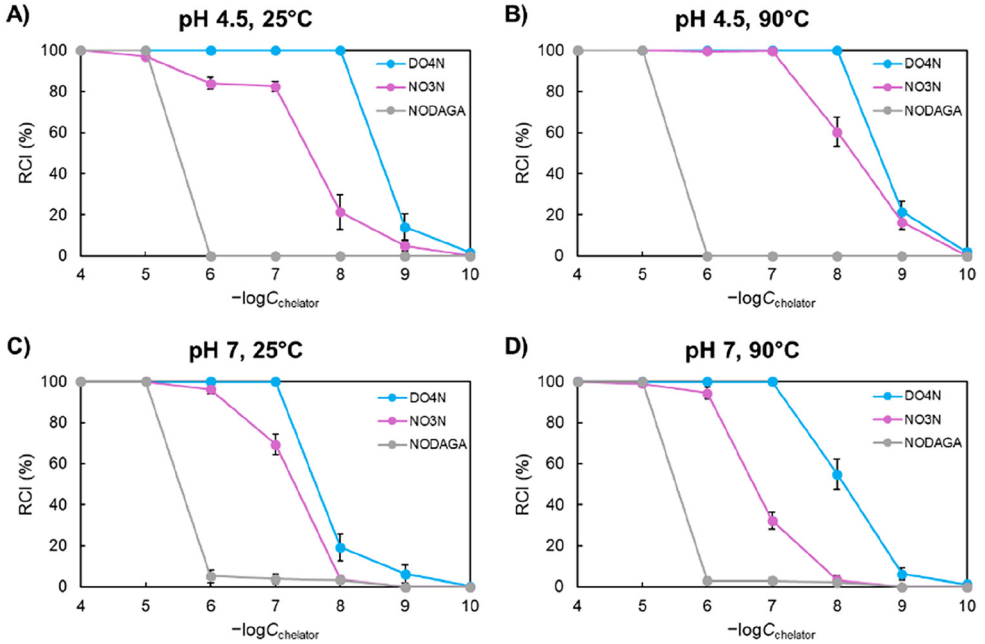

Fig. 8 Concentration-dependent radiochemical incorporation of [^{64}Cu]Cu^{2+} by DO4N, NO3N, and NODAGA at (A) pH 4.5 and T = 25 °C, (B) pH 4.5 and T = 90 °C, (C) pH 7 and T = 25 °C, (D) pH 7 and T = 90 °C (t = 10 min; 2–3 MBq ^{64}Cu, C_{Cu} = 2–3 × 10^{-9} M).

Human serum stability of [^{64}Cu]Cu^{2+} complexes with all-nitrogen macrocycles

The *in vitro* stability of [^{64}Cu]Cu-DO4N and [^{64}Cu]Cu-NO3N was assessed by incubating the complexes in human serum (1/1 *v*/*v*) alongside [^{64}Cu]Cu-NODAGA as reference. No detectable release of [^{64}Cu]Cu^{2+} was observed over time, with all complexes remaining quantitatively intact for up to 24 h (Fig. S39), a time corresponding to around two half-lives of ^{64}Cu. These findings underscore the remarkable kinetic inertness of these complexes and support further investigation of their *in vivo* stability.

Stability of [^{64}Cu]Cu-DO4N in healthy mice

Considering the encouraging *in vitro* results of DO4N and its superior performance within all the investigated aspects in comparison to NO3N and NODAGA, we considered DO4N as the most promising candidate for future clinical applications and evaluated the *in vivo* stability of its [^{64}Cu]Cu^{2+} complex in healthy mice using time-dependent PET imaging. Representative scans at various time points are shown in Fig. 9. Following intravenous injection of [^{64}Cu]Cu-DO4N, PET images revealed rapid accumulation of radioactivity in the kidneys and bladder at early time points (t < 60 min), consistent with renal clearance, as expected for highly hydrophilic small molecules. At later times (t ≥ 2 h post-injection, p.i.), kidney uptake decreased significantly, while liver accumulation became visible. This may reflect a gradual release of [^{64}Cu]Cu^{2+}, which is known to localize into the liver[4,15,38–40] or, alternatively, metabolism of the complex with hepatic accumulation of its degradation products.

Even assuming the worst-case scenario, in which the complex undergoes dissociation at longer time points, the stability of [^{64}Cu]Cu-DO4N over the first 1–2 h appears sufficient for imaging applications, which are typically performed within 1 h p.i. Importantly, this study assessed the *in vivo* behavior of the free complex; when DO4N will be conjugated to a tumor-targeting vector, its biodistribution and metabolic fate are expected to change. In such scenarios, the fast tumor uptake of the vector would likely outcompete metabolic clearance, allowing safe and effective deposition of the radioactivity at the tumor site. Therefore, the observed stability of [^{64}Cu]Cu-DO4N supports its potential utility as a chelator for radiopharmaceutical applications.

Experimental

General

All reagents and solvents were purchased from commercial suppliers (Sigma-Aldrich, Chematech, Merck, Emsure, Carlo Erba) and used without further purification. $CuCl_2{\cdot}2H_2O$ (≥99.99% trace metal basis, Aldrich) was used as the source of natural Cu^{2+}. Ultrapure water (18.2 MΩ cm) was obtained through a Purelab Chorus (Veolia) system.

Thin layer chromatography (TLC) was performed either on aluminum plates coated with silica gel 60 F_{254} (Merck) or on plastic plates coated with neutral aluminum oxide 60 F_{254} (Merck). The stationary phase for flash column chromatography was either silica gel (high-purity grade, 60 Å, 230–400 mesh, 40–63 μm, Merck) or aluminum oxide 90 active neutral (activity stage I, 0.063–0.200 mm, 70–230 mesh ASTM, Merck).

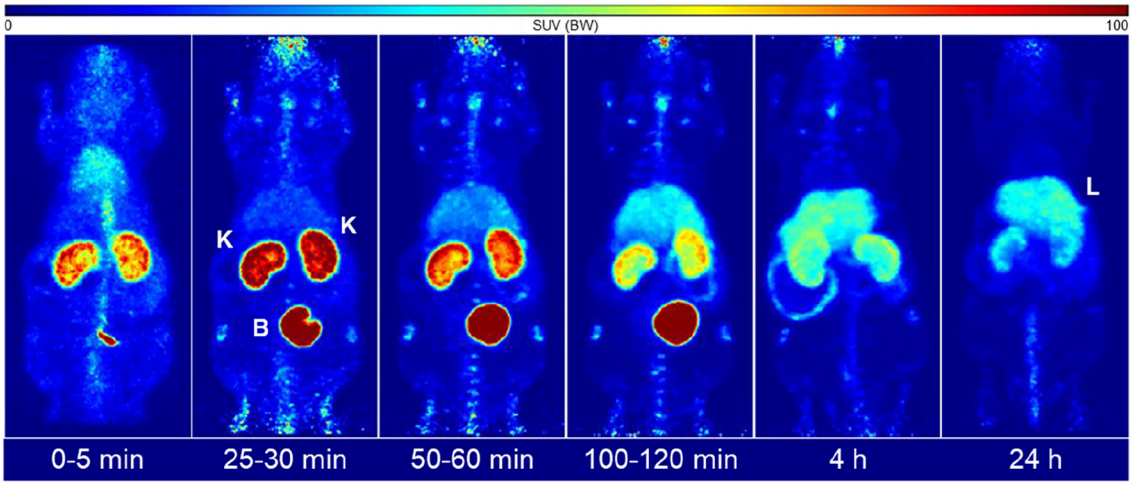

Fig. 9 Representative time-dependent (0–24 h) PET imaging of [^{64}Cu]Cu-DO4N in a healthy male NMRI nude mouse (~15 MBq [^{64}Cu]Cu-DO4N in 0.2 mL of 0.9% NaCl injected *via* tail vein catheter). K = kidney, B = bladder, L = liver.

NMR spectra were recorded with either a Bruker Avance III HD 400 (400 MHz), a Bruker Avance III 500 (500 MHz), or a Bruker Avance NEO 600 (600 MHz) spectrometer. Chemical shift (δ) is expressed in parts per million (ppm), scalar coupling constants (J) are given in Hz, and multiplicity is abbreviated as follows: singlet (s), triplet (t), multiplet (m), broad (br). ^{1}H and ^{13}C NMR spectra were calibrated relative to the residual proton solvent peak and to the ^{13}C solvent peak in the case of deuterated solvents, and relative to 3-(trimethylsilyl) propionic acid sodium salt (TSP, δ = 0 ppm) in the case of H_2O/D_2O mixed solvent.

For the quantification of Cl^-, ionic chromatography was performed with a Dionex ICS-5000$^+$ DP chromatographer equipped with a Dionex ICS-5000$^+$ DC conductivity detector (Thermo Scientific). The column (Dionex IonPac AS11-HC, 2 × 250 mm) was thermostated at 30 °C and the eluent was 85% H_2O + 15% 0.1 M NaOH (0.3 mL min^{-1}). Electrochemical regeneration was performed with a 75 mA current in a Dionex ADRS 600 (2 mm) suppressor (Thermo Scientific).

Synthesis

***tert*-Butyl-*N*-(2-chloroethyl)carbamate (3).** 2-Chloroethylamine hydrochloride (**1**) (1.00 g, 8.62 mmol, 1 eq.) was dissolved in anhydrous chloroform (20 mL). Di-*tert*-butyl dicarbonate (**2**) (1.88 g, 8.62 mmol, 1 eq.) and triethylamine (4.8 mL, 34.44 mmol, 4 eq.) were added under magnetic stirring and N_2 flow. The mixture was stirred at RT under a N_2 atmosphere overnight (o/n). A saturated NaCl aqueous solution (30 mL) was added, and the mixture was extracted with chloroform (3 × 50 mL). The organic phase was dried with Na_2SO_4, filtered and evaporated under reduced pressure. The crude was purified by flash column chromatography (silica gel, petroleum ether/ethyl acetate 90/10) to obtain **3** (800 mg, 4.45 mmol, 51% yield) as a colorless oil. ^{1}H NMR ($CDCl_3$, 500 MHz, 25 °C): 1.44 (9 H, s, CH_3), 3.45 (2 H, m, CH_2NH), 3.58 (2 H, t, J = 5.6 Hz, CH_2Cl), 4.97 (1 H, br s, NH). ^{13}C{^{1}H} NMR ($CDCl_3$, 126 MHz, 25 °C): 28.5 (CH_3), 42.6 (CH_2NH), 44.4 (CH_2Cl), 79.9 (quaternary C), 155.8 (C═O).

DO4N-Boc (5)

Cyclen (**4**) (100 mg, 0.58 mmol, 1 eq.), 3 (625 mg, 3.48 mmol, 6 eq.) and K_2CO_3 (400.8 mg, 2.90 mmol, 5 eq.) were suspended in anhydrous CH_3CN (5 mL). The mixture was stirred at 60 °C under a N_2 atmosphere for 8 d. K_2CO_3 was removed by centrifugation and the supernatant was evaporated under reduced pressure. The crude was purified by flash column chromatography (neutral alumina, CH_2Cl_2/CH_3OH, gradient from 100/0 to 98/2) to obtain **5** (234 mg, 0.31 mmol, 54% yield) as a white solid. ^{1}H NMR ($CDCl_3$, 500 MHz, 25 °C): 1.37 (36 H, s, CH_3), 2.41 (8 H, m, NCH_2CH_2NH), 2.54 (16 H, s, ring NCH_2), 3.12 (8 H, m, CH_2NH), 5.88 (4 H, br s, NH). ^{13}C{^{1}H} NMR ($CDCl_3$, 126 MHz, 25 °C): 28.5 (CH_3), 38.5 (CH_2NH), 54.1 (ring NCH_2), 54.5 (NCH_2CH_2NH), 78.9 (quaternary C), 155.9 (C═O). ESI-MS: m/z $[M + H]^+$: 746 (found); 745.56 (calc. for $[C_{36}H_{73}N_8O_8]^+$).

DO4N (6)

12 M HCl (312 µL, 3.74 mmol, 12 eq.) and CH_3OH (6 mL) were added to **5** (234 mg, 0.31 mmol, 1 eq.). The mixture was stirred at RT for 5 h, then the solvent was removed under reduced pressure to quantitatively obtain DO4N·8HCl (**6**) (141.4 mg) as a white solid. ^{1}H NMR (D_2O, 500 MHz, 25 °C, pH ~ 7): 2.90 (16 H, s, ring NCH_2), 2.95 (8 H, t, J = 7.2 Hz, $NCH_2CH_2NH_2$), 3.16 (8 H, t, J = 7.2 Hz, $NCH_2CH_2NH_2$). ^{13}C{^{1}H} NMR (D_2O, 126 MHz, 25 °C, pH ~ 7): 35.2 ($NCH_2CH_2NH_2$), 49.5 (ring NCH_2), 51.2 ($NCH_2CH_2NH_2$). HR-ESI-MS: m/z $[M + H]^+$: 345.3448 (found); 345.35 (calc. for $[C_{16}H_{41}N_8]^+$).

NO3N-Boc (8)

TACN (**7**) (91 mg, 0.70 mmol, 1 eq.), 3 (547.9 mg, 3.0 mmol, 4 eq.) and K_2CO_3 (483.7 mg, 3.5 mmol, 5 eq.) were suspended in anhydrous CH_3CN (5 mL). The mixture was stirred at 60 °C under a N_2 atmosphere overnight. K_2CO_3 was removed by fil-

tration, and the organic layer was evaporated under reduced pressure. The crude was purified by flash column chromatography (neutral alumina, CH_2Cl_2/CH_3OH, gradient from 100/0 to 90/10) to obtain **8** (264 mg, 0.47 mmol, 67% yield) as a light-yellow oil. ^{1}H NMR ($CDCl_3$, 400 MHz, 25 °C): 1.43 (27 H, s, CH_3), 2.63 (6 H, br s, N$CH_2$$CH_2$NH), 2.69 (12 H, s, ring NCH_2), 3.18 (6 H, s, CH_2NH), 5.57 (3 H, br s, NH). ^{13}C{^{1}H} NMR ($CDCl_3$, 101 MHz, 25 °C): 28.6 (CH_3), 29.8 (CH_2NH), 39.0 (ring NCH_2), 56.9 (N$CH_2$$CH_2$NH), 57.86 (quaternary C), 156.17 (C═O). ESI-MS: m/z [M + H]$^+$: 559.53 (found); 559.42 (calc. for $[C_{27}H_{55}N_6O_6]^+$).

NO3N (9)

12 M HCl (110 μL, 1.32 mmol, 12 eq.) and CH_3OH (2 mL) were added to **8** (60 mg, 0.11 mmol, 1 eq.). The mixture was stirred at RT overnight, then the solvent was removed under reduced pressure to obtain NO3N·6HCl (**9**) (42 mg, 0.09 mmol, 82% yield) as a yellow-white solid. ^{1}H NMR (D_2O, 400 MHz, 25 °C): 3.44–3.46 (24 H, m, NCH_2). ^{13}C{^{1}H} NMR (D_2O, 101 MHz, 25 °C): 34.3 ($NCH_2CH_2NH_2$), 49.6 (ring NCH_2), 52.5 ($NCH_2CH_2NH_2$). ESI-MS: m/z [M + H]$^+$: 259.3 (found); 259.26 (calc. for $[C_{12}H_{31}N_6]^+$).

Potentiometry

Variable-pH potentiometric titrations of DO4N ($C_{DO4N} \sim 10^{-3}$ M) and Cu^{2+}-DO4N ($C_{DO4N} = C_{Cu} \sim 10^{-3}$ M) were carried out as described in our previous works.[41,42] To avoid sluggish kinetics, titrations of Cu^{2+}-DO4N started at pH ∼ 3. The thermodynamic data were elaborated with HyperQuad and PITMAP as described in previous publications.[41–45] The equilibrium constants for Cu^{2+} hydroxides were taken from the literature[46] and were considered in all thermodynamic calculations.

NMR spectroscopy

Variable-pH ^{1}H NMR titrations of DO4N ($C_{DO4N} \sim 10^{-3}$ M) were carried out as described in our previous works.[41] The thermodynamic data were elaborated with the software OriginPro 2024 as described in previous publications.[41–47]

UV-Vis spectroscopy

UV-Vis spectra were acquired in the wavelength range 200–800 nm with a Cary 60 spectrophotometer (Agilent) equipped with 1 cm optical path length quartz cuvettes.

Kinetics of Cu^{2+} complexes formation

To a solution containing the ligand ($C_{L,\ final} = 10^{-4}$ M, L = DO4N or NO3N) in appropriate buffers (pH 0 by 1 M HCl, pH 1 by 0.1 M HCl, pH 2 by 0.01 M HCl, pH 3 by 10^{-3} M HCl, pH 4 by 0.01 M acetic acid/acetate buffer, pH 7.4 by 0.01 M 4-(2-hydroxyethyl)-1-piperazineethanesulfonic acid – HEPES buffer), $CuCl_2$ ($C_{Cu,\ final} = 10^{-4}$ M) was added. The electronic spectra were recorded immediately upon Cu^{2+} addition and monitored for up to ∼20 h at T = 25 °C. To ensure equilibrium was reached, the spectra of all samples were also re-acquired after heating at T = 65 °C until no further changes were observed.

Thermodynamic stability of Cu^{2+}-DO4N

pH-dependent UV-Vis titrations. Variable-pH UV-Vis spectra of Cu^{2+}-DO4N were obtained as described in our previous works.[27,31,35]

Competitive titrations with cyclen. Batch solutions containing a fixed concentration of $CuCl_2$ and DO4N ($C_{Cu} = C_{DO4N} = 2 \times 10^{-4}$ M) were prepared. To these solutions of pre-formed Cu^{2+}-DO4N complex, increasing amounts of cyclen (C_{cyclen} = 0–2.4×10^{-4} M by 2×10^{-5} M intervals) were added. The reactions were carried out in 0.1 M HEPES (pH 7.34). UV-Vis spectra were acquired after overnight heating at T = 65 °C, and this procedure was repeated until no appreciable spectral changes could be detected, indicating equilibrium. Data were elaborated with PITMAP software.[45]

EPR spectroscopy

Batch EPR titrations of Cu^{2+} complexes were performed in the pH range 2–12. Solutions containing $CuCl_2$ (C_{Cu} = 2.0 mM) and the ligand (either DO4N or NO3N, C_L = 2.2 mM) were prepared in ultrapure water (I = 0.15 M NaCl). NaOH and HCl solutions were used to adjust the pH. For room temperature spectra, capillaries were filled with the samples. For frozen solution spectra, the samples (200 μL) were transferred into EPR tubes and CH_3OH (50 μL) was added to avoid crystallization of water upon freezing. The tubes were inserted into a dewar containing liquid nitrogen (77 K). Continuous wave EPR (CW-EPR) spectra were recorded with a Bruker EleXsys E500 spectrometer (9.54 GHz microwave frequency, 13 mW microwave power, 5 G modulation amplitude, 100 kHz modulation frequency).

The spectra were analyzed with the "epr" program.[48] Room temperature spectra were corrected by subtracting the background spectrum of pure water and were simulated using the isotropic parameters g_0, A_0 copper hyperfine coupling (I_{Cu} = 3/2) and four linewidth parameters. Frozen solution spectra were simulated using either axial ($g_\perp$, $g_\parallel$, $A_\perp$, $A_\parallel$) or rhombic (g_x, g_y, g_z, A_x, A_y, A_z) g-tensor and copper hyperfine tensor. Linewidths were fitted with orientation-dependent linewidth parameters (α, β, γ) through $\sigma_{M_I} + \alpha + \beta_{M_I} + \gamma M_I^2$, where M_I denotes the magnetic quantum number of Cu^{2+} ion. Since natural $CuCl_2$ was used for the measurements, the spectra were calculated by the summation of ^{63}Cu and ^{65}Cu spectra weighed by the respective natural abundance.

Single-crystal X-Ray diffraction

Light blue single crystals of $[Cu(H_2DO4N)Cl]Cl_3$ + solvent (**10**) were obtained by slow evaporation of a water/ethanol solution containing a 1/1 mixture of DO4N and $CuCl_2$ at pH ∼ 6. A suitable crystal was selected, mounted on a loop and transferred to the goniometer. X-ray diffraction data were collected at 100 ± 1 K on a Bruker D8 VENTURE diffractometer using MoK_α radiation. Within Olex2 software,[49] the structure was solved with the olex2.solve structure solution program[50] using Charge Flipping and refined with the olex2.refine refinement package[50] using Gauss-Newton minimization. Refinement of non-hydrogen atoms was carried out with anisotropic tempera-

ture factors, while hydrogen atoms were placed into geometric positions. They were included in structure factor calculations but were not refined. The isotropic displacement parameters of the hydrogen atoms were approximated from the *U*(eq.) value of the atom they were bonded to.

The complex was refined over two disordered positions with a chemical occupancy ratio of 0.50/0.50 and two side chains were further split into two positions with occupancy of 0.25 for each conformer. Some ethanol solvent molecules could not be localized and were considered using the solvent mask function of Olex2.[49] A solvent mask was calculated and 280 electrons were found in a volume of 606 Å^3 voids per unit cell. This is consistent with the presence of 10 ethanol and 2 water molecules which accounts for 280 electrons per unit cell.

The graphical representation and the edition of CIF files were carried out with Mercury[51] and enCIFer[52] software. Crystallographic data were deposited with the Cambridge Crystallographic Data Centre (CCDC Deposition Number 2468463).

Cyclic voltammetry

Cyclic voltammetry (CV) measurements were performed using an Autolab PGSTAT-30 (Eco Chemie, trecht, The Netherlands) potentiostat, under the control of GPES software. A three-electrode cell composed of glassy carbon (GC) (Metrohm) as the working electrode, Pt wire as the counter-electrode, and Ag/AgCl/KCl 3 M (Amel) as the reference electrode was used. The GC electrode was cleaned by mechanical abrasion with 0.05 μm alumina powder and washed in ethanol/water solution before use. All CVs were performed at ambient temperature in aqueous 0.15 M $NaNO_3$ at $C_{Cu} = 1.0 \times 10^{-3}$ M, $C_L = 1.2 \times 10^{-3}$ M (L = DO4N or NO3N) and pH 7.4, with scan rates ranging from 5 to 200 mV s^{-1}. In the potential range explored (−0.7–0 V for DO4N, −0.1–0.5 V for NO3N), the solvent with the supporting electrolyte and the free ligands were found to be electroinactive.

Radiochemistry

Caution! ^{64}Cu emits ionizing radiation. It should be handled only by trained personnel in properly equipped facilities.

[^{64}Cu]Cu^{2+} production and separation

^{64}Cu was produced at Helmholtz-Zentrum Dresden-Rossendorf (Germany) through the ^{64}Ni(p,n)^{64}Cu reaction and was isolated as [^{64}Cu]$CuCl_2$ in ∼0.05 M HCl according to already published procedures.[53,54]

[^{64}Cu]Cu^{2+} radiolabeling

Stock solutions (10^{-2} M) and serial dilutions (10^{-3}–10^{-9} M) of the chelators (DO4N, NO3N, and NODAGA as a reference) were prepared in metal-free ultrapure water. Solutions for radiolabeling were prepared by mixing an appropriate buffer (80 μL of either 0.1 M sodium acetate - final pH 4.5, or PBS 1× - final pH 7), ligand stock solution (10 μL, final concentration $C_L = 10^{-4}$–10^{-10} M) and [^{64}Cu]Cu^{2+} (10 μL, 2–3 MBq, corresponding to final $C_{Cu} \sim 2$–3×10^{-9} M). A negative control (free [^{64}Cu]Cu^{2+}) was performed by substituting the ligand with an equal volume (10 μL) of H_2O. The reaction mixture was incubated at either RT or 90 °C. RCI was determined after 10 min by radio-TLC, which was carried out over aluminum plates coated with silica gel 60 RP-18 F_{254}s (Merck) using a 0.1 M aqueous solution of sodium citrate as eluent. Under these conditions, [^{64}Cu]Cu-DO4N and [^{64}Cu]Cu-NO3N are retained at the base ($R_f = 0$), [^{64}Cu]Cu-NODAGA moves with $R_f \sim 0.7$, while free [^{64}Cu]Cu^{2+} moves with the eluent front ($R_f = 1$). Radio-TLC were analyzed with an Amersham Typhoon 5 equipped with phosphor imaging plates (GE Healthcare) and RCI was determined with the program AIDA 5.10. To confirm the TLC data, selected samples were checked also by radio-HPLC (Hewlett Packard Series 1200) equipped with a Ramona radioactivity detector (Raytest) and a ZORBAX 300SB-C18 column (250 × 4.6 mm, 5 μm particle size, Agilent). The eluent was a mixture of H_2O (0.1% trifluoroacetic acid - TFA, eluent A) and CH_3CN (0.1% TFA, eluent B) with the following gradient (A/B): 3 min 95/5, 20 min from 95/5 to 5/95, 5 min 5/95, 3 from 5/95 to 95/5, 9 min 95/5, at a constant flow rate of 1 mL min^{-1}.

In vitro stability of [^{64}Cu]Cu^{2+} complexes

For stability assay, a pre-formed [^{64}Cu]Cu^{2+} complex (50 μL) was diluted with human serum (50 μL) and its integrity was checked by radio-TLC after 10, 30 min, 1, 18, 24 h at $T = 37$ °C, as described above. A negative control was performed by diluting free [^{64}Cu]Cu^{2+} in human serum, using the same conditions as for the complexes. Any [^{64}Cu]Cu^{2+} transchelated with serum proteins migrated with solvent front ($R_f \sim 1$), while intact radiometal complex remained at its characteristic R_f (see above). The percentage of intact complex was determined by integrating the areas under the curves corresponding to the free and intact species.

Animal experiments

Animal experiments were performed at Helmholtz-Zentrum Dresden-Rossendorf (Germany) according to the guidelines of the German Regulations for Animal Welfare. The protocols were approved by the local Ethical Committee for Animal Experiments (DD24.1-5131/449/49).

Radiolabeling was carried out similarly to the procedure described above by mixing buffer (170 μL of 0.5 M sodium acetate, pH 6), DO4N stock solution (20 μL, final concentration $C_{DO4N} = 10^{-5}$ M), and [^{64}Cu]Cu^{2+} in ∼0.05 M HCl (10 μL, ∼200 MBq ^{64}Cu) at 90 °C. The final reaction volume was 200 μL.

Small animal PET was performed as described in a published procedure[55] using a nanoScan PET/CT scanner (Mediso Medical Imaging Systems, Budapest, Hungary). In brief, male NMRI nude mice (Rj:NMRI-Foxn1$^{nu/nu}$, Janvier) were anesthetized (10% desflurane in 0.5 L min^{-1} oxygen/air, 1/4 v/v) and received ∼15 MBq [^{64}Cu]Cu-DO4N (in 0.2 mL of 0.9% NaCl) *via* tail vein catheter. Positron emission data were acquired continuously for the dedicated time points (dynamic PET scan 0–120 min p.i., static PET scan at 4 and 24 h p.i.). PET data

were reconstructed using Mediso Tera-Tomo™ 3D iterative reconstruction. Images were post-processed and analyzed using ROVER (ABX) and displayed as maximum intensity projections (MIPs) at the indicated time points and scaling.

Conclusions

Copper radioisotopes, including $^{61/64/67}$Cu, represent a unique true theranostic family, offering a spectrum of radionuclides suitable for the combination of PET imaging, β^- therapy, and SPECT follow-up using chemically identical radiopharmaceuticals. Despite decades of research on copper coordination chemistry, the search for chelators that optimally balance thermodynamic stability, kinetic inertness, and bioconjugation potential continues to be a central challenge in the development of next-generation radiopharmaceuticals.

Capitalizing on the well-known binding affinity of copper for nitrogen donors, we investigated a cyclen-based chelator functionalized with aminoethyl side chains (DO4N) alongside its TACN-derived analogue (NO3N). Both chelators formed Cu^{2+} complexes with high thermodynamic stability, comparable to or exceeding that of conventional analogues containing carboxylic pendants (DOTA and NOTA). In particular, DO4N demonstrated to form the most stable Cu^{2+} complexes. Complexation kinetics were strongly pH-dependent, proceeding rapidly within minutes at mildly acidic to neutral pH and slowing down at more acidic pH due to proton competition. Structural analyses in solution and in the solid state revealed that all tertiary macrocyclic amines coordinate the metal, while only one or two primary amines of the side chains participate in binding. Cu^{2+} is encapsulated in an elongated octahedral (DO4N) or distorted square pyramidal (NO3N) geometry. Cyclic voltammetry experiments demonstrated the ability of both ligands to stabilize Cu^{+} upon reduction, underscoring their exceptional redox robustness.

Radiolabeling studies with [^{64}Cu]Cu^{2+} showed that DO4N and NO3N outperform NODAGA under all tested conditions, achieving quantitative incorporation even under mild, biologically compatible conditions. Both [^{64}Cu]Cu^{2+} complexes remained fully intact in human serum, confirming their exceptional kinetic inertness. *In vivo* PET imaging with [^{64}Cu]Cu-DO4N in healthy mice demonstrated adequate short-term stability for imaging applications, with renal clearance dominating early biodistribution.

Beyond stability, the structural features of these chelators present a distinct advantage: the uncoordinated primary amines can be exploited for conjugation to biologically active targeting vectors enabling selective delivery of copper radioisotopes to cancer cells while preserving metal binding. This combination of rapid and mild radiolabeling, high stability and inertness, redox resistance, and modular conjugation potential positions establish DO4N and NO3N as highly promising platforms for theranostic radiopharmaceutical development. Future studies in tumor-bearing animal models will focus on bioconjugates derived from these chelators to evaluate targeted radiotherapy and imaging efficacy with copper radioisotopes.

Author contributions

S. Franchi: data curation, formal analysis, investigation, methodology, writing – original draft; M. Asti: investigation, methodology, funding acquisition, resources, supervision, writing – review & editing; N. V. May: investigation, methodology, funding acquisition, resources, writing – review & editing; S. Pozzo: investigation; S. Gama: investigation, methodology, funding acquisition, resources, supervision, writing – review & editing; E. Ferrari: funding acquisition, resources, supervision, writing – review & editing; L. Pigani: investigation, writing – review & editing; C. Jentschel: investigation; C. Neuber: investigation; F. Mancin: resources, supervision; S. Stadlbauer: resources, supervision, writing – review & editing; K. Kopka: investigation, resources, supervision, writing – review & editing; C. Mamat: investigation, resources, supervision, writing – review & editing; H. Mäcke: resources, funding acquisition; V. Di Marco: funding acquisition, supervision, writing – review & editing; M Tosato: conceptualization, data curation, formal analysis, investigation, methodology, project administration, writing – review & editing.

Conflicts of interest

There are no conflicts to declare.

Data availability

The authors confirm that the data supporting the findings of this study are available within the article and its supplementary information (SI). Supplementary information: supplementary discussion about the formation kinetics of Cu^{2+} complexes with DO4N and NO3N and the solid-state structure of Cu^{2+}-DO4N; NMR (^{1}H, ^{13}C{^{1}H}, COSY, HSQC) and MS characterization of DO4N-Boc, DO4N, NO3N-Boc, and NO3N; HR-MS of Cu^{2+}-DO4N; pH-dependent ^{1}H NMR titration of DO4N; speciation plots of DO4N and NO3N; UV-Vis formation kinetics of Cu^{2+}-DO4N and Cu^{2+}-NO3N; pH-dependent UV-Vis titration of Cu^{2+}-DO4N and competition with cyclen; EPR spectra of Cu^{2+}-DO4N and Cu^{2+}-NO3N; color of Cu^{2+}-DO4N and Cu^{2+}-NO3N solutions; comparison of the UV-Vis spectra of Cu^{2+}-DO4N, Cu^{2+}-cyclen, Cu^{2+}-DOTA, Cu^{2+}-NO3N, Cu^{2+}-TACN and Cu^{2+}-NOTA; proposed solution structures of Cu^{2+}-DO4N and $[Cu(HNO3N)]^{3+}$; additional crystallographic data for $[Cu(H_2DO4N)Cl]Cl_3$; radio-TLC of [^{64}Cu]Cu-DO4N and [^{64}Cu]Cu-NO3N and radio-HPLC chromatogram of [^{64}Cu]Cu-DO4N; stability of [^{64}Cu]Cu-DO4N, [^{64}Cu]Cu-NO3N and [^{64}Cu]Cu-NODAGA in human serum; spectroscopic parameters of several Cu^{2+} complexes (PDF). See DOI: **https://doi.org/10.1039/d6qi00856a**.

CCDC 2468463 contains the supplementary crystallographic data for this paper.[56]

Acknowledgements

Part of this work was supported by the National Research, Development and Innovation Office – NKFIA (Hungary)

through the project 2021-4.1.2-NEMZ_KI-2022-00016, by COST Action CA18202 (Network for Equilibria and Chemical Thermodynamics Advanced Research – NECTAR) through a Short-Term Scientific Mission (STSM) Grant, by the Portuguese funding agency Fundação para a Ciência e a Tecnologia (FCT), and by the European Regional Development Fund (FEDER, "Regional Program of Lisbon") through the project LISBOA2030-FEDER-00786200.

The authors thank Dr Magdalena K. Blei, Dr Carsten Wolf, Dr Giordano Zanoni, Francesco Dian, Giacomo Franco, and Arianna Ramponi for their contribution.

References

1 D. L. Bailey, J. L. Humm, A. Todd-Pokropek and A. van Aswegen, *Nuclear Medicine Physics: A Handbook for Teachers and Students*, International Atomic Energy Agency, Vienna, 2014.
2 T. I. Kostelnik and C. Orvig, Radioactive Main Group and Rare Earth Metals for Imaging and Therapy, *Chem. Rev.*, 2019, **119**, 902–956.
3 IAEA Nuclear Data Services, **https://www-nds.iaea.org/**, accessed Sept. 6, 2025.
4 Copper-64 Radiopharmaceuticals: Production Quality Control and Clinical Applications, *IAEA Radioisot. Radiopharm. Ser.*, 2022, **7**, 1–125.
5 C. E. Housecroft and A. G. Sharpe, *Inorganic Chemistry, 4th ed*, Pearson, 2012.
6 E. Boros and A. B. Packard, Radioactive Transition Metals for Imaging and Therapy, *Chem. Rev.*, 2019, **119**, 870–901.
7 P. Kręcisz, K. Stefańska, J. Studziński, M. Pitucha, A. Czylkowska and P. Szymański, Radiocopper in Radiopharmacy and Medical Use: Current Status and Perspective, *J. Med. Chem.*, 2025, **68**, 2356–2376.
8 T. J. Wadas, E. H. Wong, G. R. Weisman and C. J. Anderson, Coordinating Radiometals of Copper, Gallium, Indium, Yttrium, and Zirconium for PET and SPECT Imaging of Disease, *Chem. Rev.*, 2010, **110**, 2858–2902.
9 Z. Yu, G. Blade, B. S. Bouley, I. T. Dobrucki, L. W. Dobrucki and L. M. Mirica, Coordination Chemistry of Sulfur-Containing Bifunctional Chelators: Toward *in Vivo* Stabilization of ^{64}Cu PET Imaging Agents for Alzheimer's Disease, *Inorg. Chem.*, 2023, **62**, 20820–20833.
10 R. H. Holm, P. Kennepohl and E. Solomon, Structural and Functional Aspects of Metal Sites in Biology, *Chem. Rev.*, 1996, **96**, 2239–2314.
11 K. S. Woodin, K. J. Heroux, C. A. Boswell, E. H. Wong, G. R. Weisman, W. Niu, *et al.*, Kinetic Inertness and Electrochemical Behavior of Copper(II) Tetraazamacrocyclic Complexes: Possible Implications for *In Vivo* Stability, *Eur. J. Inorg. Chem.*, 2005, **23**, 4829–4833.
12 P. Baberwal, S. Sonavane and S. Basu, The Current Status and Promising Potential of Copper-based Radiopharmaceutical Development Towards Future Theranostics: An Overview, *Nucl. Med. Commun.*, 2025, **46**, 781–792.
13 G. Gasser, L. Tjioe, B. Graham, M. J. Belousoff, S. Juran, M. Walther, *et al.* Synthesis, Copper(II) Complexation, ^{64}Cu-Labeling, and Bioconjugation of a New Bis(2-pyridylmethyl) Derivative of 1,4,7-Triazacyclononane, *Bioconjugate Chem.*, 2008, **19**, 719–730.
14 S. Juran, M. Walther, H. Stephan, R. Bergmann, J. Steinbach, W. Kraus, *et al.* Hexadentate Bispidine Derivatives as Versatile Bifunctional Chelate Agents for Copper(II) Radioisotopes, *Bioconjugate Chem.*, 2009, **20**, 347–359.
15 T. B. Bernabeu, R. Mansi, L. Del Pozzo, S. Zanger, R. H. Gaonkar, L. McDougall, *et al.* ^{61}Cu-PSMA–Targeted PET for Prostate Cancer: From Radiotracer Development to First-in-Human Imaging, *J. Nucl. Med.*, 2024, **65**, 1427–1434.
16 L. A. Bass, M. Wang, M. J. Welch and C. J. Anderson, *In Vivo* Transchelation of Copper-64 from TETA-Octreotide to Superoxide Dismutase in Rat Liver, *Bioconjugate Chem.*, 2000, **11**, 527–532.
17 FDA, Detectnet Prescribing Information, **https://www.accessdata.fda.gov/drugsatfda_docs/label/2020/213227s000lbl.pdf**, accessed Sept. 6, 2025.
18 H. S. Chong, S. Mhaske, M. Lin, S. Bhuniya, H. A. Song, M. W. Brechbiel, *et al.* Novel Synthetic Ligands for Targeted PET Imaging and Radiotherapy of Copper, *Bioorg. Med. Chem. Lett.*, 2007, **17**, 6107–6110.
19 R. A. De Silva, S. Jain, K. A. Lears, H. S. Chong, C. S. Kang, X. Sun, *et al.* Copper-64 Radiolabeling and Biological Evaluation of Bifunctional Chelators for Radiopharmaceutical Development, *Nucl. Med. Biol.*, 2012, **39**, 1099–1104.
20 H. Cai, J. Fissekis and P. S. Conti, Synthesis of Novel Bifunctional Chelator Ambasar Based on Sarcophagine for Peptide Conjugation and ^{64}Cu Radiolabelling, *Dalton Trans.*, 2009, **27**, 5395–5400.
21 N. M. Di Bartolo, A. M. Sargeson, T. M. Donlevy and S. V. Smith, Synthesis of a New Cage Ligand, SarAr, and its Complexation with Selected Transition Metal Ions for Potential Use in Radioimaging, *J. Chem. Soc., Dalton Trans.*, 2001, **15**, 2303–2309.
22 M. S. Cooper, M. T. Ma, K. Sunassee, K. P. Shaw, J. D. Williams, R. L. Paul, *et al.* Comparison of ^{64}Cu-Complexing Bifunctional Chelators for Radioimmunoconjugation: Labeling Efficiency, Specific Activity, and *In Vitro*/*In Vivo* Stability, *Bioconjugate Chem.*, 2012, **23**, 1029–1039.
23 L. Tei, A. Bencini, A. J. Blake, V. Lippolis, A. Perra, B. Valtancoli, *et al.* Coordination Chemistry of Amino Pendant Arm Derivatives of 1,4,7-Triazacyclononane, *Dalton Trans.*, 2004, **13**, 1934–1944.
24 L. Dai, W. S. Lo, Y. Gu, Q. Xiong, K.-L. Wong, W.-M. Kwok, *et al.* Breaking the 1,2-HOPO Barrier with a Cyclen Backbone for more Efficient Sensitization of Eu(III) Luminescence and Unprecedented Two-Photon Excitation Properties, *Chem. Sci.*, 2019, **10**, 4550–4559.

25 L. Tei, G. Baum, A. J. Blake, D. Fenske and M. Schröder, Lanthanide Complexes of a New Nonadentate Ligand Derived from 1,4,7-Triazacyclononane: Synthesis, Structural Characterisation and NMR Spectroscopic Studies, *J. Chem. Soc., Dalton Trans.*, 2000, **16**, 2493–2499.
26 A. Bianchi, M. Micheloni and P. Paoletti, Thermodynamic Aspects of the Polyazacycloalkane Complexes with Cations and Anions, *Coord. Chem. Rev.*, 1991, **110**, 17–113.
27 M. Tosato, M. Dalla Tiezza, N. V. May, A. A. Isse, S. Nardella, L. Orian, *et al.*, Copper Coordination Chemistry of Sulfur Pendant Cyclen Derivatives: An Attempt to Hinder the Reductive-Induced Demetalation in $^{64/67}$Cu Radiopharmaceuticals, *Inorg. Chem.*, 2021, **60**, 11530–11547.
28 G. Anderegg, F. Arnaud-Neu, R. Delgado, J. Felcman and K. Popov, Critical Evaluation of Stability Constants of Metal Complexes of Complexones for Biomedical and Environmental Applications, *Pure Appl. Chem.*, 2005, **77**, 1445–1495.
29 S. Lacerda, M. P. Campello, I. C. Santos, I. Santos and R. Delgado, Study of the Cyclen Derivative 2-[1,4,7,10-Tetraazacyclododecan-1-yl]-Ethanethiol and its Complexation Behaviour Towards *d*-Transition Metal Ions, *Polyhedron*, 2007, **26**, 3763–3773.
30 C. F. G. C. Geraldes, M. P. M. Marques, B. De Castro and E. Pereira, Study of Copper(II) Polyazamacrocyclic Complexes by Electronic Absorption Spectrophotometry and EPR Spectroscopy, *Eur. J. Inorg. Chem.*, 2000, **3**, 559–565.
31 M. Tosato, S. Franchi, A. A. Isse, A. Del Vecchio, G. Zanoni, A. Alker, *et al.* Is Smaller Better? Cu^{2+}/Cu^{+} Coordination Chemistry and Copper-64 Radiochemical Investigation of a 1,4,7-Triazacyclononane-Based Sulfur-Rich Chelator, *Inorg. Chem.*, 2023, **62**, 20621–20633.
32 A. Glasner and K. R. S. Asher, A Violet Water-soluble Copper Cyanide, *J. Chem. Soc.*, 1949, 3296–3299.
33 A. Bevilacqua, R. I. Gelb, W. B. Hebard and L. J. Zompa, Equilibrium and Thermodynamic Study of the Aqueous Complexation of 1,4,7-Triazacyclononane-*N*,*N*′,*N*″-triacetic Acid with Protons, Alkaline-Earth-Metal Cations, and Copper(II), *Inorg. Chem.*, 1987, **26**, 2699–2706.
34 B. Hathaway, M. Duggan, A. Murphy, J. Mullane, C. Power, A. Walsh, *et al.* The Stereochemistry and Electronic Properties of Fluxional Six-Coordinate Copper(II) Complexes, *Coord. Chem. Rev.*, 1981, **36**, 267–324.
35 M. Tosato, M. Pelosato, S. Franchi, A. A. Isse, N. V. May, G. Zanoni, *et al.* When Ring Makes the Difference: Coordination Properties of Cu^{2+}/Cu^{+} Complexes with Sulfur-Pendant Polyazamacrocycles for Radiopharmaceutical Applications, *New J. Chem.*, 2022, **46**, 10012–10025.
36 P. V. Bernhardt, R. Bramley, R. J. Geue, S. F. Ralph and A. M. Sargeson, An Expanded Cavity Hexaamine Cage for Copper(II), *Dalton Trans.*, 2007, **12**, 1244–1249.
37 M. T. Ma, J. A. Karas, J. M. White, D. Scanlon and P. S. Donnelly, A New Bifunctional Chelator for Copper Radiopharmaceuticals: A Cage Amine Ligand with a Carboxylate Functional Group for Conjugation to Peptides, *Chem. Commun.*, 2009, **22**, 3237–3239.
38 M. Yu, H. Qing, H. Guojian, Z. Shu, W. Wenqing, H. Youfeng, *et al.* Biodistribution of $[^{64}Cu]Cu^{2+}$ and Variance of Metallothionein during Tumor Treatment by Copper, *Nucl. Med. Biol.*, 1998, **25**, 111–116.
39 H. A. Williams, S. Robinson, P. Julyan, J. Zweit and D. Hastings, A Comparison of PET Imaging Characteristics of Various Copper Radioisotopes, *Eur. J. Nucl. Med. Mol. Imaging*, 2005, **32**, 1473–1480.
40 K. Kjærgaard, T. D. Sandahl, K. Frisch, K. H. Vase, S. Keiding, H. Vilstrup, *et al.* Intravenous and Oral Copper Kinetics, Biodistribution and Dosimetry in Healthy Humans Studied by $[^{64}Cu]$copper PET/CT, *EJNMMI Radiopharm. Chem.*, 2020, **5**, 15.
41 S. Franchi, M. Asti, M. Blei, S. Pozzo, A. Madabeni, C. Graiff, *et al.*, Heavy Alkaline Earth Radiometals for Cancer Theranostics: Coordination and Radiochemistry of Radium-223 and Barium-131 with Kryptofix 22-Based Chelators, *Inorg. Chem.*, 2025, **64**, 22422–22440.
42 M. Tosato, M. Verona, R. Doro, M. Dalla Tiezza, L. Orian, A. Andrighetto, *et al.* Toward Novel Sulphur-Containing Derivatives of Tetraazacyclododecane: Synthesis, Acid-Base Properties, Spectroscopic Characterization, DFT Calculations, and Cadmium(II) Complex Formation in Aqueous Solution, *New J. Chem.*, 2020, **44**, 8337–8350.
43 Hyperquad, **https://www.hyperquad.co.uk/**, accessed Sept. 6, 2025.
44 P. Gans, A. Sabatini and A. Vacca, To Improve Accuracy of the Calculated pK_a Values, *Ann. Chim.*, 1999, **89**, 45–49.
45 V. Di Marco, PhD Thesis, University of Padova, 1998.
46 C. F. J. Baes and R. E. Mesmer, *The Hydrolysis of Cations*, Wiley-Interscience, New York, 1976.
47 S. Franchi, A. Madabeni, M. Tosato, S. Gentile, M. Asti, L. Orian, *et al.* Navigating through the Coordination Preferences of Heavy Alkaline Earth Metals: Laying the Foundations for ^{223}Ra- and $^{131/135m}$Ba-Based Targeted Alpha Therapy and Theranostics of Cancer, *J. Inorg. Biochem.*, 2024, **256**, 112569.
48 A. Rockenbauer and L. Korecz, Automatic Computer Simulations of ESR Spectra, *Appl. Magn. Reson.*, 1996, **10**, 29–43.
49 O. V. Dolomanov, L. J. Bourhis, R. J. Gildea, J. A. K. Howard and H. Puschmann, OLEX2: A Complete Structure Solution, Refinement and Analysis Program, *J. Appl. Crystallogr.*, 2009, **42**, 339–341.
50 L. J. Bourhis, O. V. Dolomanov, R. J. Gildea, J. A. K. Howard and H. Puschmann, The Anatomy of a Comprehensive Constrained, Restrained Refinement Program for the Modern Computing Environment - Olex2 Dissected, *Acta Crystallogr., Sect. A:Found. Adv.*, 2015, **71**, 59–75.
51 C. F. Macrae, P. R. Edgington, P. McCabe, E. Pidcock, G. P. Shields, R. Taylor, *et al.*, Mercury: Visualization and Analysis of Crystal Structures, *J. Appl. Crystallogr.*, 2006, **39**, 453–457.
52 F. H. Allen, O. Johnson, G. P. Shields, B. R. Smith and M. Towler, CIF applications. XV. enCIFer: A Program for Viewing, Editing and Visualizing CIFs, *J. Appl. Crystallogr.*, 2004, **37**, 335–338.

53 M. Kreller, S. A. Brühlmann, T. Knieß, K. Kopka and M. Walther, Production of Medical Radionuclides in the Center for Radiopharmaceutical Tumor Research - A Status Report, *Instruments*, 2024, **8**, 1–15.
54 S. Thieme, M. Walther, H. J. Pietzsch, J. Henniger, S. Preusche, P. Mäding, *et al.* Module-Assisted Preparation of ^{64}Cu with High Specific Activity, *Appl. Radiat. Isot.*, 2012, **70**, 602–608.
55 L. R. Loureiro, L. Hoffmann, C. Neuber, L. Rupp, C. Arndt, A. Kegler, *et al.* Immunotheranostic Target Modules for Imaging and Navigation of Unicar T-Cells to Strike FAP-Expressing Cells and the Tumor Microenvironment, *J. Exp. Clin. Cancer Res.*, 2023, **42**, 341.
56 CCDC 2468463: Experimental Crystal Structure Determination, 2026, DOI: **10.5517/ccdc.csd.cc2nvmv0**.